RESEARCH ARTICLE

Disabled Homolog 2 Controls Prometastatic Activity of Tumor-Associated Macrophages

Ilaria Marigo[1], Rosalinda Trovato[2], Francesca Hofer[2], Vincenzo Ingangi[1], Giacomo Desantis[1], Kevin Leone[1], Francesco De Sanctis[2] ,Stefano Ugel[2], Stefania Canè[2], Anna Simonelli[2], Alessia Lamolinara[3], Manuela Iezzi[3], Matteo Fassan[4], Massimo Rugge[4], Federico Boschi[5], Giulia Borile[6,7], Thomas Eisenhaure[8], Siranush Sarkizova[8], David Lieb[8], Nir Hacohen[8], Luca Azzolin[9], Stefano Piccolo[9,10], Rita Lawlor[11], Aldo Scarpa[11,12], Luisa Carbognin[13], Emilio Bria[13], Silvio Bicciato[14], Peter J. Murray[15], and Vincenzo Bronte[2]

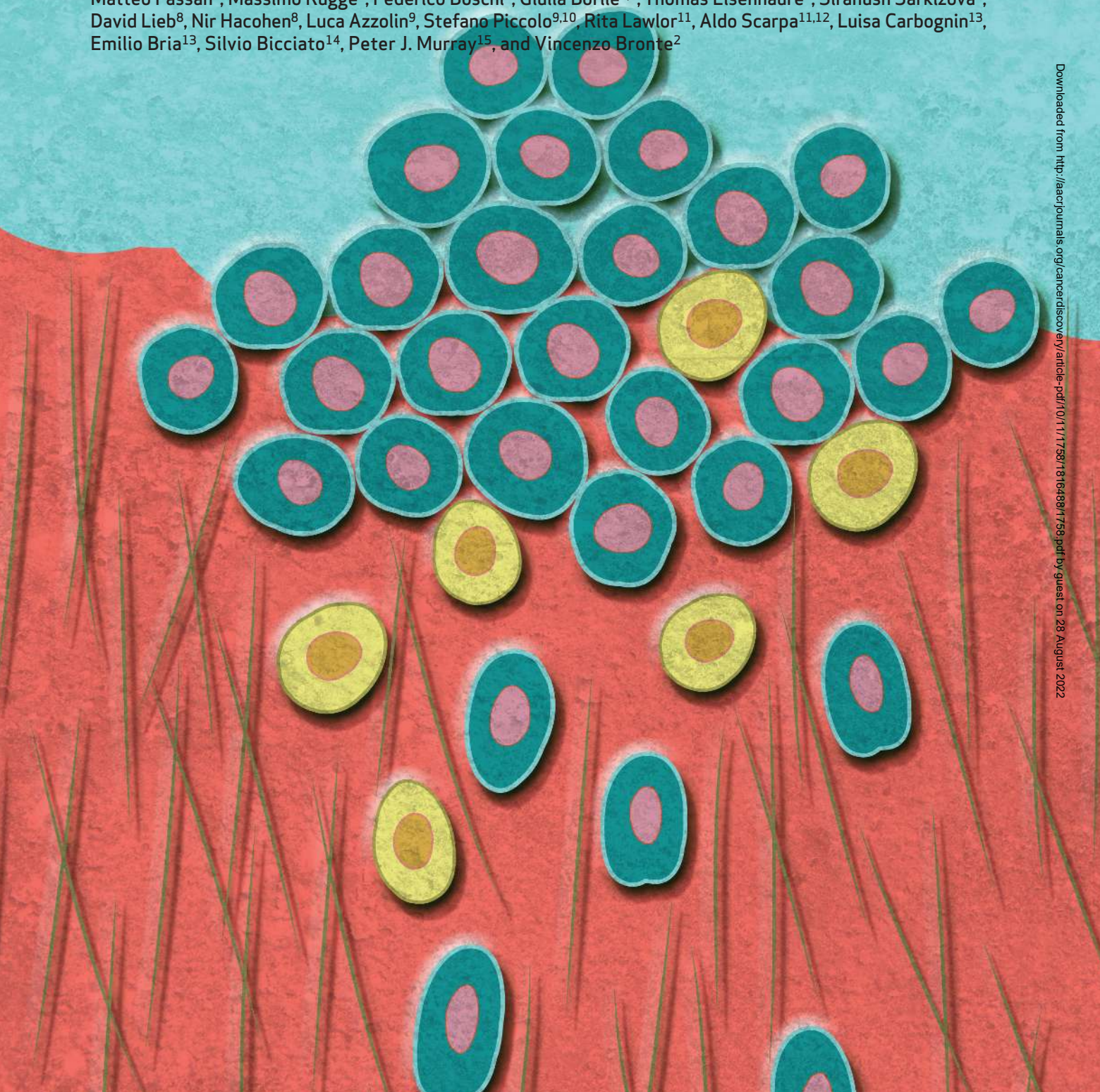

ABSTRACT Tumor-associated macrophages (TAM) are regulators of extracellular matrix (ECM) remodeling and metastatic progression, the main cause of cancer-associated death. We found that disabled homolog 2 mitogen-responsive phosphoprotein (DAB2) is highly expressed in tumor-infiltrating TAMs and that its genetic ablation significantly impairs lung metastasis formation. DAB2-expressing TAMs, mainly localized along the tumor-invasive front, participate in integrin recycling, ECM remodeling, and directional migration in a tridimensional matrix. DAB2$^+$ macrophages escort the invasive dissemination of cancer cells by a mechanosensing pathway requiring the transcription factor YAP. In human lobular breast and gastric carcinomas, DAB2$^+$ TAMs correlated with a poor clinical outcome, identifying DAB2 as potential prognostic biomarker for stratification of patients with cancer. DAB2 is therefore central for the prometastatic activity of TAMs.

SIGNIFICANCE: DAB2 expression in macrophages is essential for metastasis formation but not primary tumor growth. Mechanosensing cues, activating the complex YAP–TAZ, regulate DAB2 in macrophages, which in turn controls integrin recycling and ECM remodeling in 3-D tissue matrix. The presence of DAB2$^+$ TAMs in patients with cancer correlates with worse prognosis.

INTRODUCTION

Because metastases are estimated to be responsible for about 90% of cancer-related deaths worldwide, there is an urgent need to understand the mechanisms underlying the metastatic process and identify therapeutic targets and biomarkers of metastatic disease (1). In solid cancers, tumor-associated macrophages (TAM) are abundant immune cells, and their presence correlates with a poor prognosis (2–5). TAMs exhibit tumor-supporting actions both at primary (i.e., cell invasion and intravasation) and metastatic sites (i.e., extravasation, seeding, and cell growth; refs. 6, 7). Different molecules influence the macrophage-assisted metastatic process, such as colony-stimulating factor 1 (CSF1; ref. 8) and CCL2 (6), which are mainly responsible for TAM and metastasis-associated macrophage (MAM) accumulation; however, the lack of either specific markers or molecularly defined mechanisms responsible for TAM-mediated metastasis promotion remains a limiting factor for the development of antimetastatic therapies (9).

Disabled homolog 2, mitogen-responsive phosphoprotein (DAB2) exists as two isoforms (96 or 67 kDa following post-translational modification) and is a phosphoprotein with an actin-binding *N*-terminal domain, a central conserved domain, and a proline/serine-rich *C*-terminal portion with binding sites for SH3 domains. DAB2 was initially identified in a CSF1-responsive macrophage cell line (10). Recent studies have suggested that DAB2 modulates cancer-associated RAS–MAPK (11), TGFβ (12), NFκB (13), and WNT (14) signaling. DAB2 is thought to act as an adaptor protein between cell membrane receptors and the machinery responsible for the clathrin-mediated endocytosis (CME) of membrane receptors (15, 16). Combining endocytosis with directional exocytosis, DAB2 concentrates shuttling proteins into specific sites of the cell membrane, favoring interplay with the surrounding extracellular matrix (ECM; ref. 17). Changes in ECM composition, tissue stiffness, and integrin repertoire govern cell directional migration in response to gradients of adhesive molecules and matrix rigidity, migratory processes known as haptotaxis and durotaxis, respectively (18).

The mechanisms that control ECM remodeling and cellular movement during metastatic invasion are ill-defined, primarily because information about specific molecular interactions among cells and matrix in the context of macrophage-assisted metastasis is missing. Here we unveil a fundamental and nonredundant prometastatic activity of DAB2 in TAMs. Moreover, we demonstrate the value of the gene encoding DAB2 as a potential prognostic marker for disease progression in patients, either as a single gene or in association with other tumor-promoting genes.

[1]Veneto Institute of Oncology IOV-IRCCS, Padova, Italy. [2]Department of Medicine, Section of Immunology, University of Verona, Verona, Italy. [3]Department of Medicine and Aging Science, Center for Advanced Studies and Technology (CAST), University G. D'Annunzio of Chieti-Pescara, Chieti, Italy. [4]Department of Medicine-DIMED, University of Padova, Padova, Italy. [5]Department of Computer Science, University of Verona, Verona, Italy. [6]Department of Physics and Astronomy "G. Galilei," University of Padova, Padova, Italy. [7]Institute of Pediatric Research Città della Speranza, Padova, Italy. [8]Broad Institute of MIT and Harvard, Cambridge, Massachusetts. [9]Department of Molecular Medicine, University of Padova, Padova, Italy. [10]IFOM, The FIRC Institute for Molecular Oncology, Padova, Italy. [11]ARC-Net Centre for Applied Research on Cancer, University and Hospital Trust of Verona, Verona, Italy. [12]Department of Diagnostic and Public Health, University of Verona, Verona, Italy. [13]Fondazione Policlinico Universitario Agostino Gemelli IRCCS, Università Cattolica Del Sacro Cuore, Roma, Italy. [14]Department of Life Sciences, Center for Genome Research, University of Modena and Reggio Emilia, Modena, Italy. [15]Max Planck Institute for Biochemistry, Martinsried, Germany.

Note: Supplementary data for this article are available at Cancer Discovery Online (http://cancerdiscovery.aacrjournals.org/).

I. Marigo and R. Trovato contributed equally to this article.

Corresponding Authors: Vincenzo Bronte, University of Verona, P.le L.A. Scuro, 10, Verona 37134, Italy. Phone: 3904-5812-4007; Fax: 3904-5812-6455; E-mail: vincenzo.bronte@univr.it; Rosalinda Trovato, rosalinda.trovato@univr.it; and Ilaria Marigo, Veneto Institute of Oncology IOV-IRCCS, via Gattamelata 64, Padova 35128, Italy. Phone: 3904-9821-5897; E-mail: ilaria.marigo@iov.veneto.it

Cancer Discov 2020;10:1758–73

doi: 10.1158/2159-8290.CD-20-0036

RESULTS

Myeloid Cells Expressing *Dab2* Display Protumoral Features

Previous gene chip data obtained by our group on tumor-infiltrating myeloid cells isolated from different mouse tumors highlighted *Dab2* as one of the most upregulated genes. To define DAB2 expression in the tumor microenvironment (TME) and begin dissecting the effects of *Dab2* deletion in myeloid cells, we generated an autochthonous transgenic mouse model of lobular breast carcinoma, the PyMT-*Dab2*$^{flox/flox}$; *Tie2*-Cre^{+} (referred as PyMT-*Dab2* KO) strain, lacking the DAB2 protein in the entire hematopoietic lineage and a fraction of endothelial cells (19). A single-cell RNA-sequencing analysis (scRNA-seq) was performed on FACS-sorted, tumor-infiltrating myeloid cells from either PyMT-*Dab2* KO mice or their littermates [PyMT-wild type (WT)]. A total of 5,170 myeloid cells were grouped into 14 different clusters that we define as six macrophage clusters (MΦ_1-6); two monocyte clusters, Mono_1 (*Ly6c2*$^{+}$*Ccr2*$^{+}$ inflammatory monocytes, iMo) and Mono_2 (mix of iMo and *Cebpb*$^{+}$*Nr4a1*$^{+}$ patrolling monocytes, pMo); four dendritic cell (DC) clusters (*Cd209a*$^{+}$ DC_1, *Ccr7*$^{-}$ DC_2, *Cd24a*$^{+}$ DC_3 and *Ccr7*$^{+}$ DC_4); a mixed cluster of macrophages and DCs (MΦ-DC); and a cluster of PMN-like cells, which did not express the canonical neutrophil marker (i.e., *Ly6g*; Fig. 1A; Supplementary Fig. S1A and S1B; Supplementary Data S1). *Dab2* was present in almost all clusters of macrophages, in inflammatory Mono_1 class, in MΦ-DC cells, and in 2 of 4 clusters of DCs (DC_1 and DC_2; Supplementary Fig. S1C). Moreover, *Dab2* KO cells were strongly enriched in MΦ_4 and weakly enriched in MΦ_1 and MΦ_5, whereas WT cells were mainly represented in the MΦ_2 cluster (Supplementary Fig. S1D). We then analyzed the genes differentially expressed between all macrophages from WT compared with *Dab2* KO mice (Fig. 1B). Among those upregulated in WT cells, we found genes involved in tissue remodeling (*Cxcl2, Mmp12)* and promotion of M2-like phenotype (*Atf3, Fos, Jun, Klf4*; refs. 20–23). On the contrary, *Dab2* KO cells displayed an increased expression of IFN-inducible genes (*Ly6e, Ccl5, Iftm3, Ifi27l2a, Irf7*). To outline distinct macrophage states, we performed an unsupervised clustering of either WT (n = 1,682 cells) or *Dab2* KO (n = 1749 cells) macrophages separately. We identified 6 clusters of macrophages in WT (all expressing *Dab2*, Supplementary Fig. S1E) and 7 in *Dab2* KO tumors (Fig. 1C and D). On the basis of the expression levels of genes distinctive of each cluster, we classified clusters as low inflammatory (MΦ_WT0, MΦ_WT1, MΦ_WT5, MΦ_KO0, MΦ_KO1, MΦ_KO5, MΦ_KO6), mixed inflammatory (MΦ_WT2, MΦ_WT3, MΦ_KO3), and proinflammatory (MΦ_WT4, MΦ_KO2, MΦ_KO4) clusters (Fig. 1C and D; Supplementary Data S2 and S3). However, several macrophage-related processes (i.e., antigen-presenting, metabolism, heat shock response, protumoral, and others) were identified and annotated in Supplementary Data S3. Two clusters were shared by WT and KO tumors (WT2-KO3 mixed-inflammatory and WT4-KO4 IFN signature), whereas others designated only one condition, such as the antigen-presenting cluster in KO mice (MΦ_KO0) and the protumoral MΦ_WT5 cluster characterized by a *Ccl7, Ccl8*, and *Mrc1* gene signature (Fig. 1C and D). To explore relationships between clusters, we calculated theoretical trajectories for WT and *Dab2* KO macrophages based on a minimal spanning tree on the clusters. Three prospective trajectories were identified for WT macrophages, each starting from inflammatory low–mixed clusters (MΦ_WT1, MΦ_WT2, MΦ_WT3) and leading to two poorly inflammatory terminal branches, MΦ_WT0 (inflammatory inactive) and MΦ_WT5 (protumoral signature), as well as to one characterized by interferon signature (MΦ_WT4; Supplementary Fig. S1F; Supplementary Data S3). On the contrary, *Dab2* KO trajectory presented a common path starting with cells with a low/anti-inflammatory profile (MΦ_KO6 and MΦ_KO5) and reaching either strong interferon response profile (MΦ_KO4) or highly inflammatory macrophage terminal branches (MΦ_KO2; Supplementary Fig. S1F; Supplementary Data S3). Collectively, these data support the existence of unique functional states for WT and *Dab2* KO macrophages.

Myeloid Cells Expressing DAB2 Support the Metastatic Process by a Mechanism Independent from the Adaptive Immune Response

To assess the contribution of DAB2-expressing myeloid cells in tumor progression and metastatic spread, we orthotopically injected the MN-MCA1 fibrosarcoma cell line in WT and *Dab2* KO mice. *Dab2* KO mice showed a significant reduction in the number of lung metastases when compared with WT mice (Fig. 2A and B). On the contrary, there was no significant alteration in the primary tumor growth (Fig. 2C). Metastasis reduction in *Dab2* KO mice challenged with MN-MCA1 tumor cells was confirmed in the *Dab2*$^{flox/flox}$;*LysM*Cre^{+} mouse strain, which targets gene deletion in monocytes/macrophages and neutrophils (24), further consolidating the role of DAB2^{+} myeloid cells in metastatic cascade (Fig. 2D–F). We then tested the outcome of *Dab2* deficiency in breast cancer models metastasizing to the lung. WT mice, orthotopically injected with syngeneic E0771 cells, presented lung metastatic foci compared with an almost complete absence of lesions in *Dab2* KO mice (Fig. 2G and H), with a slight alteration in primary tumor growth (Fig. 2I). Similarly, in PyMT-*Dab2* KO, we found a reduction in metastasis number, area, and burden compared with their control littermates (PyMT-WT; Fig. 2J and K; Supplementary Fig. S2A and S2B), whereas primary tumor growth and tumor onset were unaltered (Fig. 2L; Supplementary Fig. S2C). *Dab2* deficiency did not induce any obvious alteration either in the immune-suppressive activity of myeloid cells as well as in the recruitment of immune cell subpopulations to the tumor mass (Supplementary Fig. S2D and S2E). Moreover, we better characterized T and natural killer (NK) cells in MN-MCA1 tumor-bearing mice. We did not detect any difference in the percentage of CD4^{+} T, CD8^{+} T, and NK cells infiltrating the primary tumors of WT and *Dab2* KO mice (Supplementary Fig. S2F), as well as in IFNγ and granzyme (GRZ) B expression in tumor-infiltrating CD8^{+} T and NK cells after a 4-hour stimulation with PMA and iomomycin (Supplementary Fig. S2G). Actually, we observed a slightly higher presence of CD4^{+}IFNγ^{+} cells in *Dab2* KO mice compared with WT mice (Supplementary Fig. S2G, left). Collectively, our results argue that tumor-infiltrating myeloid cells expressing DAB2 are responsible for tumor cell invasiveness by a mechanism independent of the immune

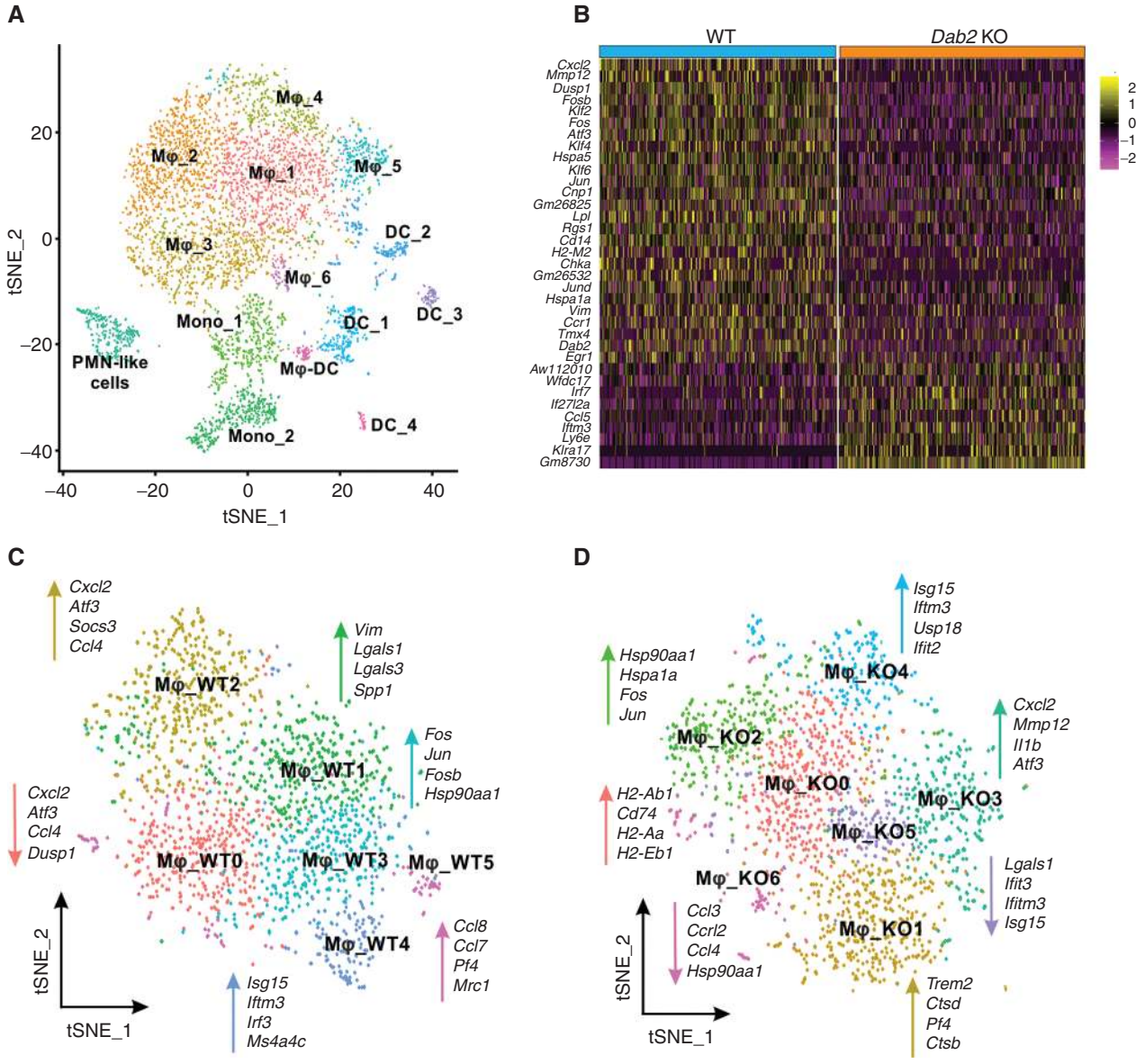

Figure 1. scRNA-seq analysis of tumor-infiltrating myeloid cells. **A,** tSNE visualization of 5,170 cells. WT and *Dab2* KO cells were clustered together. **B,** Heat map of differentially expressed genes between WT and *Dab2* KO MΦs. **C** and **D,** tSNE analysis of macrophages from WT (**C**) and *Dab2* KO (**D**) mice. Selected, enriched genes used for biological identification of each cluster are shown.

suppression of adaptive antitumor immune response against the primary tumor.

DAB2 Is Mainly Expressed by TAMs Localized along the Invasive Tumor Border

Our scRNA-seq experiment suggested that *Dab2* expression was enriched in several macrophage populations. Therefore, we evaluated the expression of DAB2 protein among different tumor-infiltrating myeloid cells using a highly specific anti-DAB2 antibody. As expected, DAB2 isoforms were detected in TAMs isolated from MN-MCA1 tumor–bearing mice, to a much lower extent in monocytes and completely absent in granulocytes (Fig. 3A; Supplementary Fig. S3A, top, and S3B). Moreover, DAB2 was expressed in TAMs sorted from PyMT primary tumors, but not in resident mammary tissue macrophages (MTM; Fig. 3B; Supplementary Fig. S3A, bottom). Within both MN-MCA1 and PyMT-WT tumors, DAB2$^+$ TAMs were mainly localized in perilesional areas at the invasive front line between the tumor and the surrounding healthy tissue, with fewer numbers in the tumor core as well as in both healthy muscle and normal breast (Fig. 3C; Supplementary Fig. S3C and S3D). The differentiation and proliferation of monocytes and macrophages is mainly controlled by CSF1 and CSF2 cytokines (25). Because both transplantable tumor cell lines secreted CSF1 (Fig. 3D), we investigated the effects of this cytokine on *Dab2* gene expression. Bone marrow (BM)–derived CD11b$^+$ cells isolated from either tumor-bearing or tumor-free mice upregulated *Dab2* mRNA when

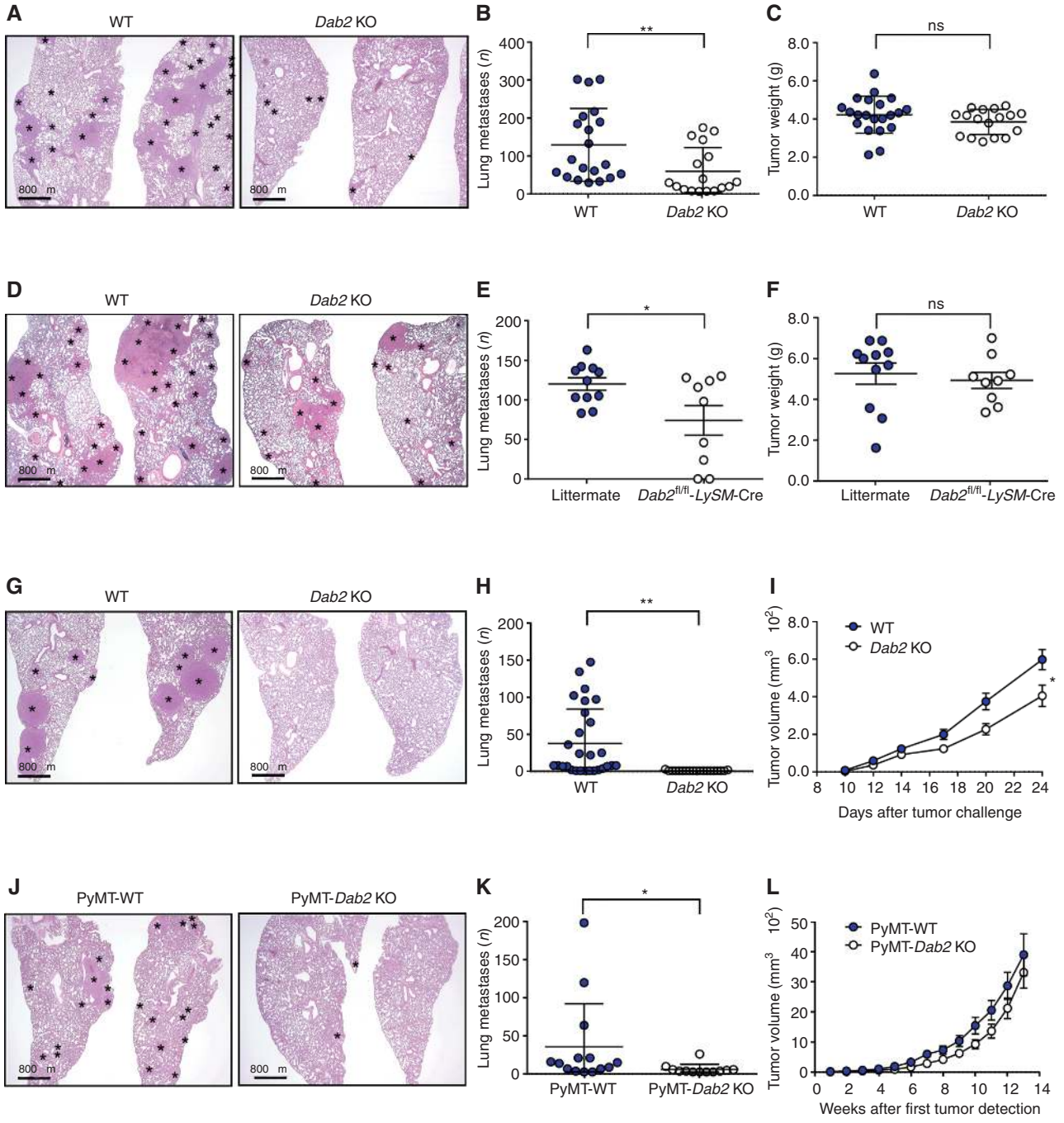

Figure 2. *Dab2* deficiency in myeloid cells affects the metastatic process. **A,** Representative hematoxylin and eosin (H&E)-stained microscopy images of the lung metastasis in either WT or *Tie2*-Cre *Dab2* KO mice orthotopically injected with MN-MCA1 fibrosarcoma cells. Scale bar, 800 μm. **B,** Quantification of lung metastases number. **C,** Primary tumor growth reported as tumor weight (g) and measured 24 days after tumor challenge. WT ($n = 20$) or *Tie2*-Cre *Dab2* KO ($n = 17$), pooled from three independent experiments. **D,** Representative H&E-stained microscopy images of the lung metastases in either *LySM*-Cre *Dab2* KO mice or their littermates, orthotopically injected with MN-MCA1 fibrosarcoma cells. Scale bar, 800 μm. **E,** Quantification of lung metastasis number. **F,** Primary tumor growth reported as tumor weight (g) and measured 24 days after tumor challenge. WT ($n = 11$) or *Dab2* KO ($n = 9$), pooled from two independent experiments. **G,** Representative H&E-stained microscopy images of the lung metastases in either WT or *Tie2*-Cre *Dab2* KO mice orthotopically injected with E0771 breast cancer cells. Scale bar, 800 μm. **H** and **I,** Number of lung metastases (**H**) and primary tumor growth over time (**I**) are reported. WT ($n = 22$) and *Dab2* KO mice ($n = 18$), pooled from three independent experiments. **J,** Representative H&E-stained microscopy images of the lung metastases in either WT or *Tie2*-Cre *Dab2* KO PyMT transgenic mice. Scale bar, 800 μm. **K,** Quantification of lung metastasis numbers by H&E staining of PyMT-WT ($n = 13$) or PyMT-*Dab2* KO ($n = 12$) mice. **L,** Tumor growth reported as tumor volume (mm^3) evaluated over time. Data are presented as mean ± SE. *, $P \leq 0.05$; **, $P \leq 0.01$; ***, $P \leq 0.001$ by Mann–Whitney test (**B**, **C**, **E**, **F**, **H**, **K**) and two-way repeated measures ANOVA (**I**, **L**).

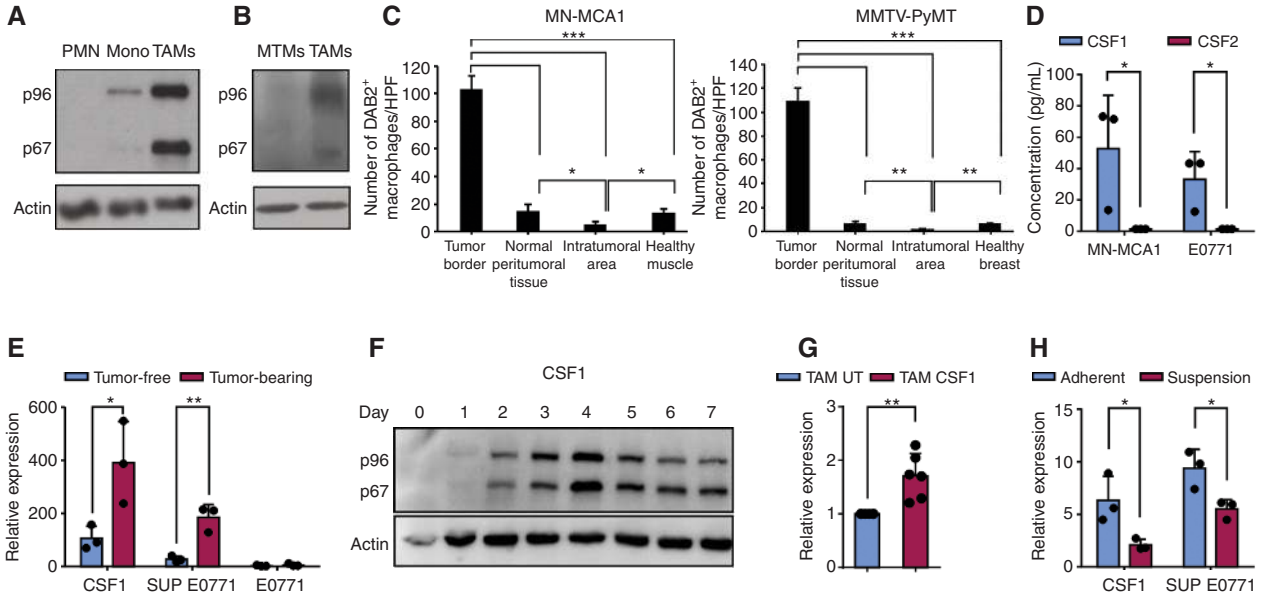

Figure 3. Tumor microenvironment induces DAB2 expression in TAMs that localize along tumor borders. **A** and **B,** Western blot analysis for DAB2 expression (p96 and p67 isoforms) on FACS-sorted myeloid cell subsets (granulocytes, monocytes, and TAMs) infiltrating primary tumors from either MN-MCA1-tumor bearing mice (**A**) or TAMs and MTMs from PyMT mice (**B**). **C,** Quantification of DAB2$^+$ TAMs on total TAMs evaluated on High Power Field (HPF) images from different areas of either MN-MCA1 (left) or PyMT tumors (right). **D,** Secretion of CSF1 and CSF2 assessed by ELISA in cancer cell supernatant ($n = 2$ independent experiments). **E,** *Dab2* expression assessed by qRT-PCR on CD11b$^+$ cells isolated from BM of tumor-free and MN-MCA1-bearing mice and cultured for 24 hours in the presence of CSF1, E0771 supernatant, or E0771 cells ($n = 3$ independent experiments). **F,** DAB2 expression evaluated by Western blot analysis on BM precursors from WT mice during differentiation with CSF1. **G,** *Dab2* expression assessed by qRT-PCR on TAMs isolated from MN-MCA1 tumor–bearing mice, cultured for 24 hours in the absence (UT) or presence of CSF1 ($n = 3$ independent experiments). **H,** *Dab2* expression assessed by qRT-PCR on CD11b$^+$ cells isolated from BM of tumor-free mice and cultured for 6 hours either as adherent cells or in suspension, in the presence of CSF1 or supernatant of E0771 cells ($n = 3$ independent experiments). **A**, **B**, and **F**, Actin was used as loading control. Data are presented as mean ± SD. *, $P \le 0.05$; **, $P \le 0.01$; ***, $P \le 0.001$ by one-way ANOVA (**C**) and Student *t* test (**D**, **E**, **G**, **H**).

exposed to either CSF1 or E0771 tumor cell supernatant but not in direct coculture with the tumor cells (Fig. 3E). The amounts of *Dab2* mRNAs were significantly higher when CD11b$^+$ cells were isolated from tumor-bearing mice (Fig. 3E). Accordingly, p96 and p67 DAB2 isoforms were increased during the CSF1-driven *in vitro* macrophage differentiation from BM precursors (Fig. 3F). *Dab2* genetic ablation in CD11b$^+$ cells did not alter macrophage differentiation and expansion (Supplementary Fig. S3E), indicating that *Dab2* is not overtly involved in CSF1-dependent signal transduction. Moreover, *Dab2* transcription was also induced by CSF1 in mature macrophages isolated from MN-MCA1 tumors (Fig. 3G).

Because *in vitro* cultures generate adherent macrophages, we addressed the interplay between cytokines and mechanical cues during *in vitro* differentiation by treating BM precursors under adherent or suspension culture conditions. *Dab2* mRNA upregulation induced by CSF1 and tumor-derived soluble factors was impaired when cells were not anchored to a solid, stiff surface (i.e., plastic), indicating that chemical and mechanical stimuli must be integrated for a full induction of *Dab2* gene in macrophages (Fig. 3H).

Integrin Recycling and ECM Remodeling Mediated by DAB2 Macrophages Promote Tumor Cell Invasion

Considering that DAB2$^+$ macrophages were localized at the tumor-invasive front, we investigated their direct participation in tumor cell spreading. E0771 breast cancer cells cocultured with WT TAMs displayed an increased invasive ability within the surrounding matrix when compared with either E0771 cells alone or cocultured with *Dab2*-deficient TAMs (Fig. 4A).

In cancer cells, DAB2 can regulate the internalization and recycling of different membrane proteins, including integrins (26), which mediate cell–ECM component interactions. To verify whether DAB2 could be involved in integrin recycling in macrophages, we evaluated the surface expression of three integrin heterodimers, α1β1, α5β1, and α6β1, which bind collagen, fibronectin, and laminin, respectively. We found that the lack of DAB2 in bone marrow–derived macrophages (BMDM) influenced α5, α6, β1, but not α1 integrin turnover, leading to their accumulation on the plasma membrane without affecting the levels of total protein and mRNA (Fig. 4B and C; Supplementary Fig. S4A). Because integrins are key regulators of diverse cell movement types (27), we examined the ability of DAB2$^+$ macrophages to migrate in response to either soluble (chemotactic) or matrix-bound (haptotactic) cues. WT or *Dab2* KO BMDMs exhibited a comparable directional movement toward chemokine gradients (Supplementary Fig. S4B), but were defective in moving through the 3-D Matrigel substrate when lacking *Dab2* (Supplementary Fig. S4C), consistent with a defect in haptotaxis, but not chemotaxis. The altered integrin surface distribution in *Dab2* KO BMDMs also impaired their ability to internalize ECM fragments (Fig. 4D), a process occurring during matrix

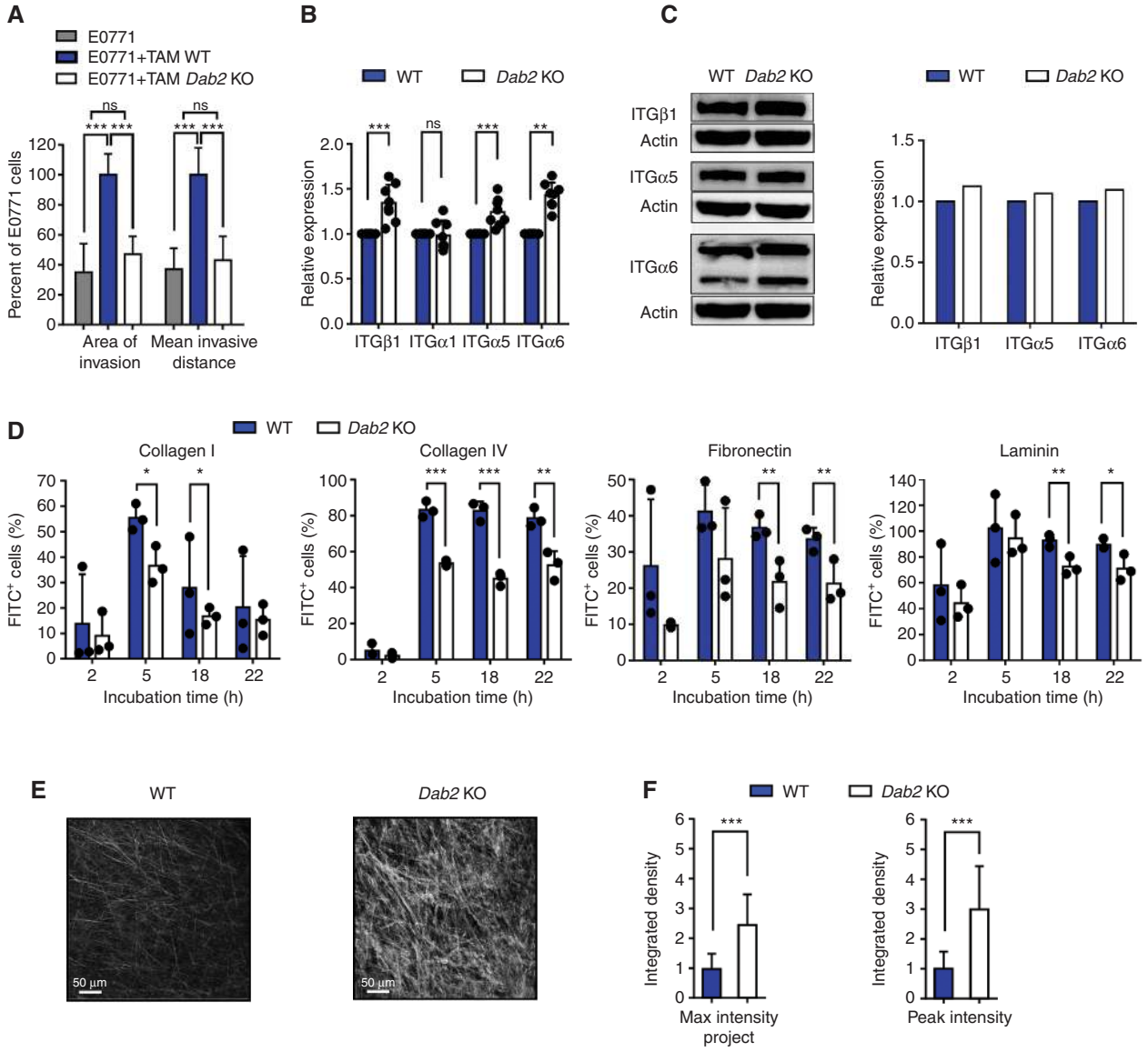

Figure 4. DAB2 regulates tissue invasion and ECM remodeling by macrophages. **A,** Inverted invasion assay of E0771 tumor cells, either alone or coincubated with TAMs isolated from WT or *Dab2* KO tumor-bearing mice. The area of invasion and the mean invasive distance of E0771 cells were evaluated by confocal microscopy ($n = 3$ independent experiments). **B,** Surface expression of integrins β1, α1, α5, and α6 evaluated by flow cytometry on either WT or *Dab2* KO BMDMs. The fold changes in mean fluorescence intensity (MFI) relative to WT is reported for each integrin ($n = 8$ independent experiments). **C,** Expression of integrins β1, α5, and α6 evaluated by Western blot analysis and densitometry on either WT or *Dab2* KO BMDMs (left). Actin was used as loading control. Densitometric quantification of Western blot bands reported as fold change over WT samples (right). **D,** Uptake of FITC-labelled ECM proteins by BMDMs is reported as percentage of FITC$^+$ cells measured by flow cytometry at different time points ($n = 3$ independent experiments). **E,** Representative SHG images of collagen fibrils organization in MN-MCA1 WT and *Dab2* KO tumors. Scale bar, 50 μm **F,** Maximum projection intensity through 0–80 μm *z*-stack of SGH signal intensity and peak intensity within MN-MCA1 (WT $n = 9$ and *Dab2* KO $n = 8$) tumors. Data are presented as mean ± SD. *, $P \le 0.05$; **, $P \le 0.01$; and ***, $P \le 0.001$ by one-way ANOVA (**A**) and Student *t* test (**B**, **D**, **F**).

remodeling (28). Accordingly, the ability of E0771 cells to invade the previously macrophage-remodeled Matrigel was compromised (Supplementary Fig. S4D), highlighting that tumor cell invasion relies on matrix reorganization through a DAB2-dependent step in macrophages. Furthermore, a second harmonic generation (SHG) analysis of primary explants of MN-MCA1 tumors confirmed that the ECM presented an organized and dense structure in tumors grown in *Dab2* KO mice compared with WT controls (Fig. 4E and F). Therefore, we conclude that *Dab2* KO macrophages have an impaired endocytosis of ECM proteins due to an altered integrin turnover, which affects the macrophage tissue-remodeling properties.

DAB2$^+$ Macrophages Favor Tumor Cell Invasion through Integrin–ECM Interaction

To dissect further the role of DAB2 in integrin-mediated remodeling of ECM, we generated different CRISPR/Cas9 clones of RAW 264.7 macrophage cell line by deleting either

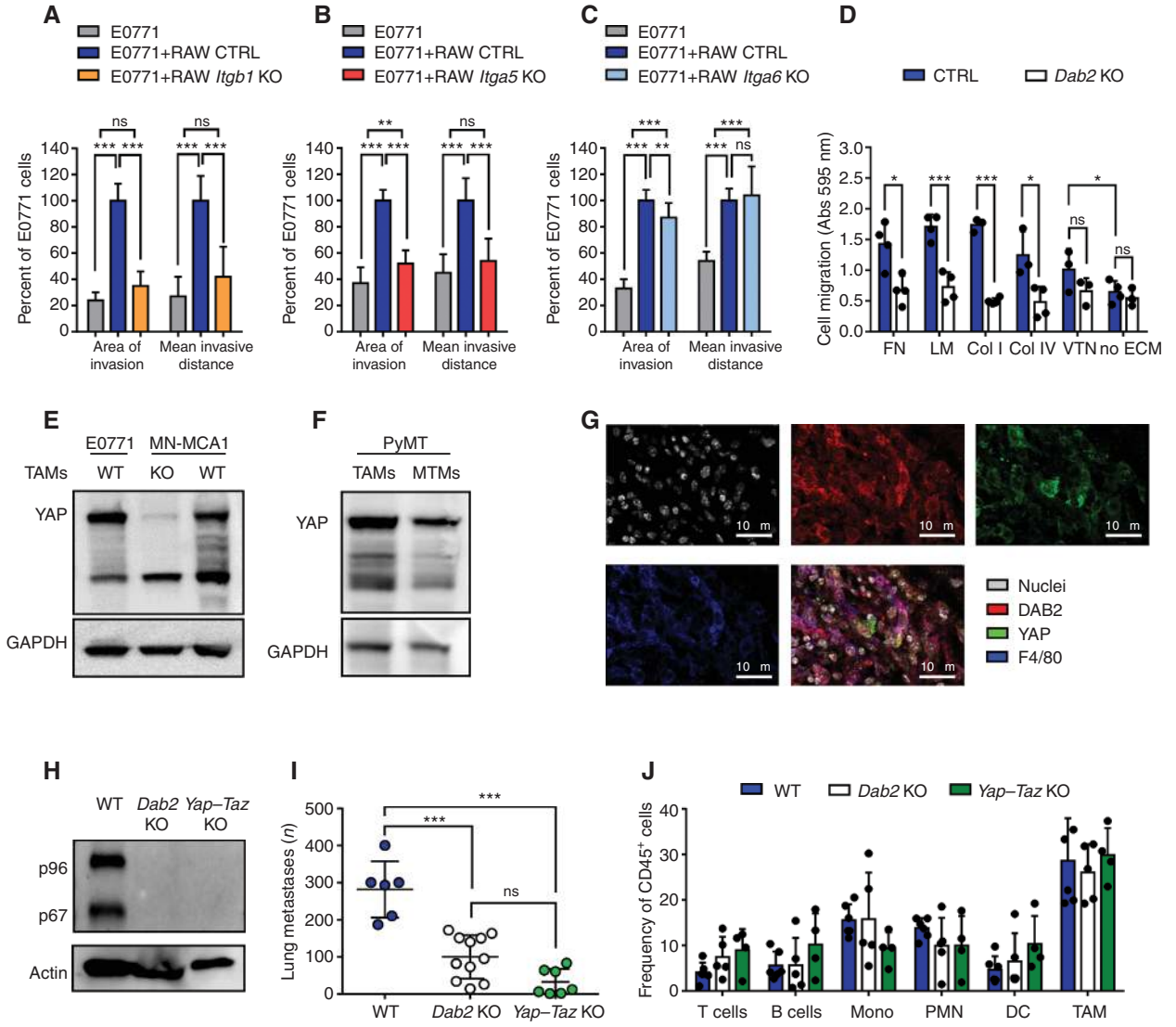

Figure 5. DAB2$^+$ macrophages favor tumor cell invasion by integrin and ECM interaction. **A–C,** Inverted *in vitro* invasion assays of RAW 264.7 CTRL or *Itgb1* (**A**), *Itga5* (**B**), and *Itga6* KO (**C**) single-cell–derived clones cocultured with E0771 tumor cells in a Matrigel layer. The area of invasion and the mean invasive distance for E0771 were quantified by confocal microscopy ($n = 2$ independent experiments). **D,** Transwell invasion assay of RAW 264.7 CTRL and *Dab2* KO single cell–derived clones using a synthetic matrix (Puramatrix) supplemented with fibronectin (1 μg/mL), laminin (1 μg/mL), collagen I (1 μg/mL), collagen IV (10 μg/mL), or vitronectin (1 μg/mL). Cell invasion was evaluated measuring the absorbance at 595 nm of crystal violet stained cells ($n = 2$ independent experiments). **E** and **F,** Western blot analysis for YAP expression on FACS-sorted TAMs from E0771 and MN-MCA1 tumor-bearing WT or KO mice (**E**) or TAMs and MTMs isolated from PyMT mice (**F**). GAPDH was used as loading control. **G,** IF performed to evaluate expression of YAP, DAB2, and F4/80 on PyMT tumor slices. Scale bar, 10 μm. **H,** Western blot analysis for DAB2 expression on TAMs isolated from MN-MCA1 tumor–bearing WT, *Dab2* KO, and *Yap–Taz* KO mice. **I,** Quantification of lung metastases in WT ($n = 6$), *Dab2* KO ($n = 11$), and *Yap–Taz* KO ($n = 7$) mice orthotopically injected with MN-MCA1 cells. **J,** Accumulation of different immune populations among CD45$^+$-gated cells in MN-MCA1 tumors from WT ($n = 6$), *Dab2* KO ($n = 5$), or *Yap–Taz* KO ($n = 4$) mice. Data are presented as mean ± SD. *, $P \le 0.05$; **, $P \le 0.01$; ***, $P \le 0.001$, by one-way ANOVA (**A–C**, **I–J**) and Student *t* test (**D**).

Dab2 or the genes encoding the integrins β1, α5, and α6 (Supplementary Fig. S5A and S5B; Supplementary Table S1). Analogous to TAMs, RAW 264.7 cells support E0771 cell invasion when expressing DAB2 (Supplementary Fig. S5C). Tumor cell invasion was reduced only when β1 and α5 were absent, but was unaffected by integrin α6 modulation (Fig. 5A–C). Accordingly, RAW 264.7 clones with the genes encoding the β1 and α5 subunits deleted, but not the gene encoding α6, displayed a reduced ability to remodel the matrix, indicating that α5β1 but not α6β1 integrin dimers are required for macrophage-assisted ECM remodeling (Supplementary Fig. S5D). DAB2 expression was similar in all the integrin KO clones (Supplementary Fig. S5E), implying that the outside-in integrin signaling is not a direct regulator of DAB2 expression, at least for the analyzed integrins.

Changes in matrix composition and structure enable integrins to transmit biochemical and mechanical signals to the interior of cells and fine-tune cell migration and invasion (29). Interestingly, RAW 264.7 WT controls, but not *Dab2*-deleted clones, displayed an increased invasive ability in the

presence of the ECM proteins that are known to interact with DAB2-regulated integrins (i.e., fibronectin, laminin, and collagen I and IV), but were unaltered when exposed to vitronectin, which binds αvβ3 integrin, a DAB2-independent dimer (Fig. 5D and data not shown). Moreover, the invasive ability of RAW 264.7 WT changed according to the ECM protein concentration, in line with studies on tissue-migrating muscle cells (30), but remained unmodified in *Dab2*-deleted clones (Supplementary Fig. S5F).

In response to mechanical inputs due to the high ECM stiffness, the mechanotransduction-related cotranscription factors YAP and TAZ regulate cell proliferation, survival and motility of cancer cells (31, 32), and activation of cancer-associated fibroblasts (33). Using a gene set enrichment analysis (GSEA) to correlate *Dab2* expression in macrophages with known molecular pathways, we found a significant relationship between DAB2- and YAP-related signature (31), in addition to the expected correlation with CSF1 signaling (Supplementary Fig. S5G). YAP was detectable in DAB2-expressing TAMs isolated from E0771, MN-MCA1, and PyMT tumors but also in MTMs that do not express DAB2, demonstrating that YAP expression is independent of DAB2 (Fig. 5E and F). Moreover, almost all the F4/80$^+$DAB2$^+$ TAMs in the stromal area at the border of the tumor mass were also YAP$^+$ (Fig. 5G; 95.7± 2.3% of the total F4/80$^+$DAB2$^+$ cells). To investigate whether *Dab2* expression was regulated by mechanotransduction, we generated (*Yap–Taz*)$^{flox/flox}$;*Tie2*-Cre$^+$ (*Yap–Taz* KO) mice. DAB2 expression was negligible in TAMs sorted from these mice, suggesting that *Dab2* transcriptional regulation is controlled by the YAP–TAZ complex *in vivo* (Fig. 5H). *Yap–Taz* KO mice challenged with MN-MCA1 cells phenocopied the *Dab2* KO mice, with a reduced number of lung metastases but without any detectable impact on either primary tumor growth (data not shown) or leukocyte infiltration (Fig. 5I and J). Furthermore, a SHG analysis performed on primary explants of MN-MCA1 tumors revealed an increased collagen fiber density in tumors grown in *Yap–Taz* KO mice compared with WT controls, mirroring the enriched ECM network unveiled in *Dab2* KO tumors (Supplementary Fig. S5H and S5I).

DAB2 Is Expressed in Metastatic Lung and Supports Lung Colonization

So far, our results indicated that DAB2$^+$ macrophages are essential for matrix remodeling and this process licenses tumor cell invasiveness. To explore whether *Dab2* expression in the hematopoietic compartment affected myeloid cell ability to reach the metastatic site, we analyzed the myeloid infiltrate in the lungs of tumor-bearing WT and *Dab2* KO mice. We found similar percentages of myeloid subpopulations (Supplementary Fig. S6A) Moreover, DAB2-expressing macrophages in MN-MCA1 tumor–bearing mice were localized inside the metastatic foci, with a peculiar distribution toward the borders (Supplementary Fig. S6B and S6C, left), whereas few DAB2-expressing macrophages were present in healthy areas of lungs (Supplementary Fig. S6C, right).

Notably, E0771 tumor cells, intravenously injected in either WT or *Dab2* KO mice, gave rise to lung metastases, but their number, mean area, and burden were significantly higher in WT mice compared with *Dab2* KO mice (Fig. 6A–C), suggesting DAB2 intervention also occurs in distal steps of metastasis development. Inflammatory monocytes can assist the extravasation of tumor cells from the blood to the lung (6). Because DAB2 was detectable at low levels in tumor-infiltrating monocytes (Fig. 3A), we evaluated their possible aid in endothelial transmigration of cancer cells. E0771 tumor cells extravasate in a similar manner through an endothelial layer in the presence of Ly6C$^+$ monocytes isolated from either WT or *Dab2* KO–tumor-bearing mice, ruling out this step in DAB2-dependent metastatic progression (Supplementary Fig. S6D). Moreover, mCherry/Luc E0771 tumor cells, intravenously injected in either WT or *Dab2* KO mice, seeded the lung in similar numbers within the first days of tumor challenge (Fig. 6D). Metastases started to be detectable, by imaging, 9 days after tumor injection in WT mice, whereas no significant luminescence was detectable in *Dab2* KO mice throughout the observation time. After 28 days, when WT mice had to be euthanized, cancer cells increased from about 10^4 to 10^6 per lung, whereas they were barely detectable in *Dab2* KO mice (Fig. 6D and E), suggesting that *Dab2* absence could favor tumor cell clearance within the metastatic lung. Interestingly, a different CD3$^+$ T-cell frequency was observed at the metastatic site, mainly dependent on a reduced percentage of CD4$^+$ T cells in *Dab2* KO mice; CD8$^+$ T- and NK-cell frequencies were unaffected (Supplementary Fig. S6E). Nevertheless, NK cells in *Dab2* KO mice displayed an activated phenotype (increased GRZB and CD107a expression along with higher expression levels of activatory receptors) that was not observed in T lymphocytes (Supplementary Fig. S6 F-I); this landscape was not mirrored at the primary tumor, suggesting that different immune contexts are established at the two sites (Supplementary Fig. S2G and data not shown). Indeed, in the absence of *Dab2* checkpoint immunotherapy with anti–PD-1 in MN-MCA1 tumor–bearing mice did not alter primary tumor growth but successfully reduced lung metastases (Fig. 6F and G). These data suggest that DAB2 is not only required for the first steps of metastatic cascade at the primary tumors, but could exert a different role in promoting cancer cell growth and invasion at the metastatic site. Moreover, checkpoint inhibitors synergize with DAB2 absence in controlling metastatic disease.

DAB2$^+$ Macrophage Presence Correlates with Worse Prognosis in Patients with Cancer

Breast cancer is a heterogeneous disease, with variability in stromal composition and TAM infiltration according to histology [invasive ductal and lobular carcinoma (IDC and ILC, respectively)] and molecular subtypes (luminal, HER2-enriched, and triple-negative; refs. 2, 34, 35). We assessed the potential prognostic role of DAB2 expression in a cohort of 32 patients with pure, early-stage ILC tumors who underwent surgery. The number of DAB2$^+$ cells with macrophage morphology was evaluated in both peritumoral and intratumoral areas (Supplementary Fig. S7A). High DAB2 levels were associated with significantly worse 10-year disease-free survival (DFS) for both peritumoral and intratumoral areas (Fig. 7A). High levels of DAB2 also associated with the presence of lymph node metastases and high tumor cell proliferation index (Ki-67) either in peritumoral and intratumoral areas (36) and with vascular

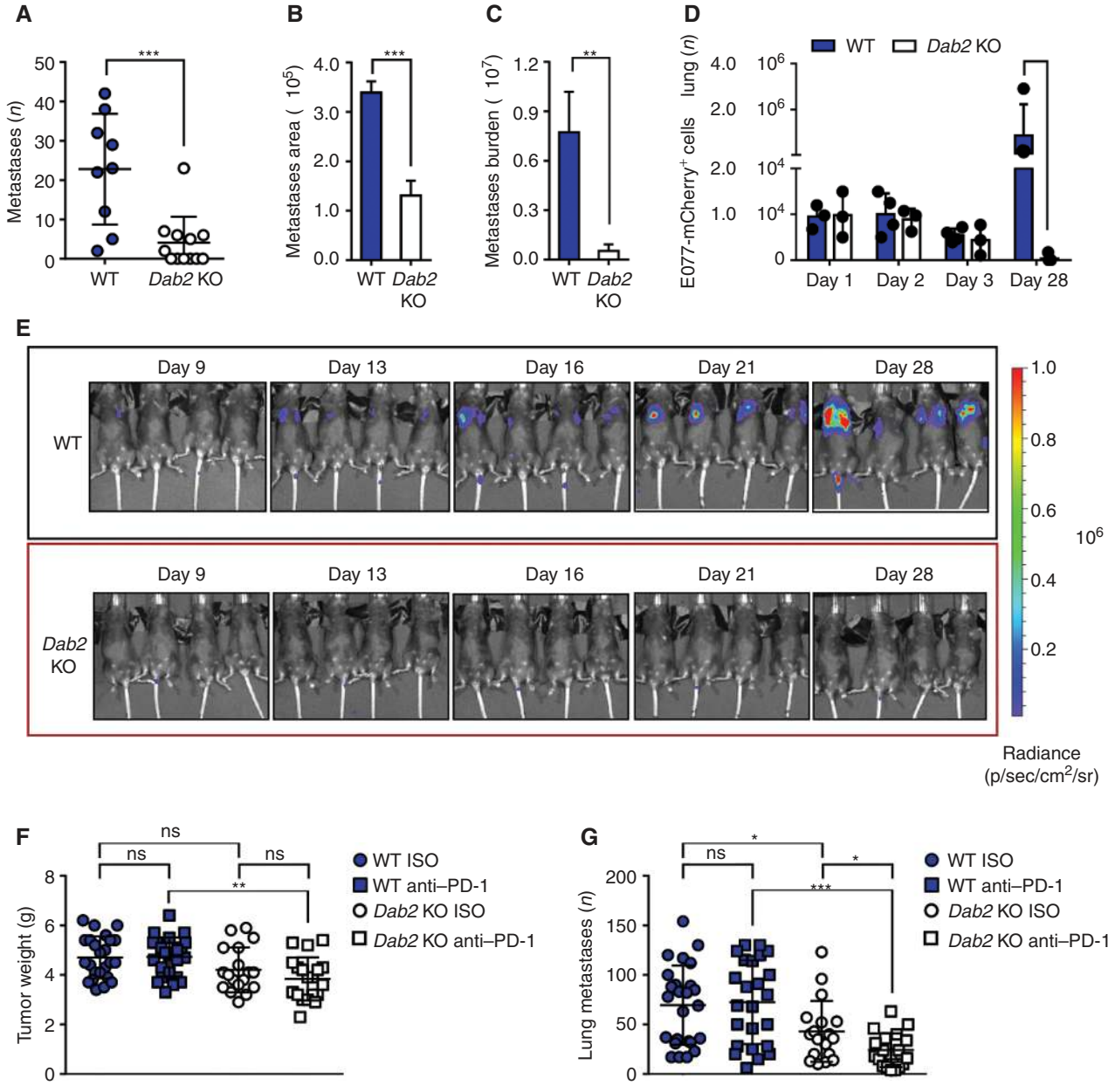

Figure 6. DAB2 expression in MAMs regulates lung colonization. **A–C,** Quantification of lung micrometastasis number (**A**), mean area (**B**), and burden (**C**) at day 20 following E0771 intravenous injection in either WT ($n = 9$) or *Dab2* KO ($n = 12$) mice. **D,** Absolute numbers of mCherry$^+$ E0771 cells per lung in WT and *Dab2* KO mice 1, 2, 3, or 28 days after tumor challenge ($n = 3$ mice/group). **E,** Metastasis formation in WT and *Dab2* KO mice following mCherry/Luc E0771-cell intravenous injection, evaluated by bioluminescence imaging. **F** and **G,** Primary tumor growth (**F**) and lung metastases evaluation (**G**) on MN-MCA1 tumor–bearing WT (ISO $n = 25$, Anti–PD-1 $n = 24$) or *Dab2* KO (ISO $n = 18$, anti–PD-1 $n = 19$) mice after immunotherapy with anti–PD-1 or its isotopic control. **A–D**, **F**, and **G**, Data are presented as mean ± SD. *, $P \le 0.05$; **, $P \le 0.01$; ***, $P \le 0.001$ by Student *t* test.

invasion in intratumoral area (Supplementary Table S2; Supplementary Fig. S7B and S7C). Thus, DAB2$^+$ macrophages at the tumor site represent a potential prognostic marker for tumor progression and metastasis formation in patients with primary resected ILC. We then explored the distribution of DAB2$^+$ macrophages in another series of luminal ILC cases as defined by current guidelines (37). We detected a significantly increased number of DAB2$^+$ macrophages, both peritumoral and intratumoral, in the luminal B patients compared with luminal A (Supplementary Table S3; Fig. 7B). Moreover, focusing only on the luminal patients in The Cancer Genome Atlas (TCGA) dataset, *DAB2* mRNA expression had a similar negative correlation with overall survival also in luminal B IDCs (Supplementary Fig. S7D). We further evaluated the clinical relevance of a two-gene signature of *DAB2* in association with some genes highlighted by the scRNA-seq of mouse samples (Fig. 1B and C) and described as protumoral (2, 21, 38). Few ILC luminal B cases are present in TCGA cohort; therefore, we focused only on

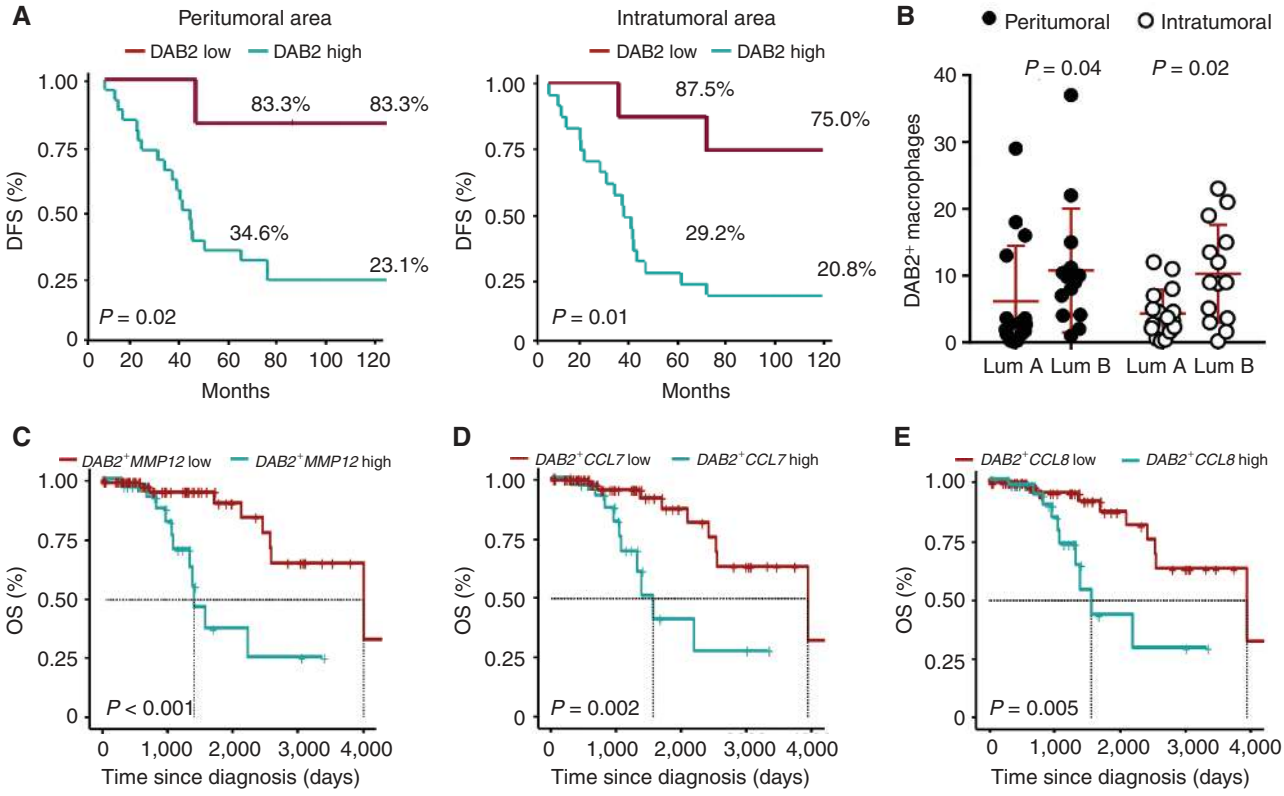

Figure 7. Prognostic value of DAB2+ TAMs in breast cancers. **A,** DFS according to peritumoral (low $n = 6$ vs. high $n = 26$, ROC-derived optimal cutoffs) or intratumoral (low $n = 8$ vs. high $n = 24$, ROC-derived optimal cutoffs) DAB2 staining in 32 patients with ILC who had undergone surgery (log-rank *P*). **B,** Peritumoral and intratumoral DAB2 levels (IHC) in patients with luminal breast cancer (Lum A = 16, Lum B = 14). **C–E,** Overall survival (OS) according to *DAB2* + *MMP12* expression (**C**), *DAB2* + *CCL7* expression (**D**), and *DAB2* + *CCL8* expression (**E**; mRNA, low vs. high) in IDC luminal B breast cancers analyzed in the TCGA database (log-rank *P*).

patients with IDC. As shown in Fig. 7C–E, high *MMP12, CCL7*, or *CCL8* in association with high *DAB2* expression strongly correlated with a poor clinical outcome, whereas single genes were not able to discriminate patients' survival (*MMP12* $P = 0.76$, *CCL7* $P = 0.45$, *CCL8* $P = 0.45$). These data highlight the presence of shared expression modules across mouse and human TMEs. Finally, we assessed the prognostic value of *DAB2* expression in other cancers. A significant inverse correlation in survival was observed between high *DAB2* mRNA expression and poor prognosis in liver and gastric cancer from TCGA dataset (Supplementary Fig. S7E). Therefore, we extended our analyses to a series of tumor samples from 59 patients affected by early-stage gastric cancer who had undergone R0 resection (Supplementary Table S4). Also, in this patient group, DAB2+ macrophages presented a heterogeneous expression among different cases. Patients with high DAB2 expression showed a reduction in 3-year cancer-specific survival (CSS) and overall survival (OS), either borderline or significant, respectively (Supplementary Fig. S7F and S7G).

DISCUSSION

Among tumor-infiltrating immune cells critical for tumor progression and metastatic spreading (39), TAMs can support tumor cell invasion and intravasation at the primary site as well as extravasation, seeding, and tumor cell growth at the metastatic niche (6, 40–42). Macrophages represent a heterogeneous cell population that consists in a continuum of different states that cannot be completely recapitulated in the bipolar M1–M2 classification. The scRNA-seq of tumor-infiltrating myeloid cells unveiled that *Dab2* deficiency can reprogram the tumor microenvironment toward a more proinflammatory status in accordance with previous studies (13, 43). However, we could not uncover any difference in M1–M2 polarization among WT and KO mice in either TAMs isolated from tumor mass or BMDMs exposed *in vitro* to polarizing signals (data not shown), which prompted us to contemplate alternative explanations for the prometastatic activity of DAB2. Indeed, we defined a novel *Dab2*-dependent, macrophage-intrinsic pathway that controls cancer dissemination. *Dab2* genetic ablation in macrophages significantly affected lung metastasis formation in sarcoma and breast cancer models without any overt variation in primary tumor growth or dysregulation of antitumor immunity. DAB2 is thus a TAM marker associated with macrophage prometastatic activity. *Dab2* upregulation was dependent on CSF1, a major determinant of mononuclear phagocyte biology (25), which has already been linked to increased tumor progression and metastases in PyMT mice (8). Notably, CSF1-induced *Dab2* upregulation in BM precursors was

optimal when cells were maintained under adherence to the plastic surface as compared with stimulation in cell suspension. CSF1 is thus necessary but not sufficient for full gene induction. Another significant and in part unexpected finding is that DAB2 deficiency ablates haptotaxis along tissue matrix, but not chemotaxis. The mechanistic foundation of this dichotomy relies on the physical interaction between cells and ECM proteins as prerequisite for ECM remodeling and local migration. DAB2$^+$ macrophages invade 3-D matrices with movements dependent on ECM protein concentration and, likely, matrix stiffness. *Dab2*-deficient cells presented a reduced integrin recycling and a consequent higher accumulation of integrins α5, α6, and β1 on their surface compared with WT cells. By genetic deletion of single integrin chains, we proved the prominent intervention of α5β1 heterodimers in DAB2-assisted promotion of tumor cell invasion. Interestingly, α5β1 heterodimers preferentially bind fibronectin, a typical component of premetastatic niche (44, 45). The absolute dependency of DAB2 in TAMs on the YAP–TAZ transcription factor complex further argues that mechanosensing cues are essential for continuous expression of the protein within tumor stroma. YAP expression is modulated by the substrate stiffness: soft matrices induce cytoplasmic retention, whereas stiff matrices cause its nuclear transfer and activation (32). To our knowledge, for the first time, this study relates DAB2 protein in macrophages to the transcriptional YAP–TAZ complex, demonstrating that DAB2 contributes to downstream events in mechanotransduction, acting as a connector between ECM stiffness and integrin recycling and functionality. DAB2$^+$ presence in tissue-resident macrophages is limited in healthy tissues; instead, DAB2$^+$ macrophages accumulated during tumor progression and localized near the invasive front where the stroma stiffness, cellular mechanosignaling, and YAP expression are the highest in human breast cancer samples (34). In patients, there is a sharp gradient of increasing matrix stiffness from the less aggressive breast cancer subtypes, that is, luminal A and B, toward the more aggressive basal-like and HER2 tumors (34). We speculate that less aggressive tumors rely on cancer-extrinsic mechanisms (DAB2$^+$ macrophages) to invade nearby tissues, whereas the epigenetic rewiring occurring in more aggressive variants might render the tumor cells less dependent on external aids. Indeed, epigenetically distinct subpopulations of breast cancer cells (defined as "trailblazer") able to guide migration of passenger cancer cells were characterized by a seven-gene signature including *DAB2*, which correlated with poor patient outcome in the triple-negative breast cancer subtype (46). This might also explain why the *DAB2* gene is predictive of overall patient survival in luminal B immunophenotype (both ILC and IDC histotypes), but not in all patients with breast cancer, as instead highlighted for gastric and hepatocellular carcinoma. The proof of concept that DAB2 protein expression in macrophages might be a biomarker for disease stratification will require further validation with the simultaneous detection of DAB2 and other known macrophage markers (i.e., CD68, CD169) and application to different molecular subtypes of breast cancer (luminal, triple negative, and HER2$^+$), as well as in tumors with different histologies. The identification of TAM markers is essential for a more refined stratification of patients with breast cancer, as recently reported for SIGLEC1 and CCL8 expression (2). Notably, the predictive role of *DAB2* as a prognostic marker for poor survival in breast cancer is amplified by the association with CCL7, a metastasis-promoting cytokine (38), CCL8, which was recently pointed out as a marker discriminating TAMs in invasive breast cancer tissue specimens (2), and MMP12, a macrophage metalloelastase involved in tissue remodeling and metastasis promotion (21). In the last few years, several macrophage-targeting drugs have been developed for depletion of (i.e., CCR2 or CSF1R antagonists), reprogramming of (i.e., PI3Kγ and HDAC inhibitors), or interference with (i.e., arginase 1) effector pathways in macrophages, and clinical trials are ongoing (9). However, all these approaches present drawbacks due to nonspecific side effects on normal macrophages. More importantly, the current cancer drug discovery route is biased to ignore the impact of new molecules and treatments for metastasis interference. Results from clinical trials in past years have not invigorated the development of antimetastatic drugs by the pharmaceutical industry (47). We have shown here that DAB2 might offer a fully new avenue for antimetastatic therapy, wholly disjoined from the primary tumor growth. Indeed, DAB2-targeted treatments might interfere with the metastatic process at different steps, operating after primary tumor resection, to cure hidden or dormant metastases also in association with immunotherapy. To fully exploit this therapeutic combination, however, a deeper understanding of the mechanisms responsible for the efficacy of anti–PD-1 therapy in controlling hematogenous metastases in *Dab2*-deficient mice, which include a characterization of NK-cell involvement, will be necessary.

METHODS

Animal Studies

Eight-week-old C57BL/6 WT mice were purchased from Charles River Laboratories Inc. *Tie2*-Cre (*Tek*-Cre) and *Dab2*$^{flox/flox}$ mice were originally provided to P.J. Murray (St. Jude Children's Research Hospital, Memphis, TN) from J.A. Cooper (Fred Hutchinson Cancer Center, Seattle, WA) and were cross-bred to generate *Dab2* KO mice. *LySM*-Cre mice were a gift from P. Scapini (University of Verona, Verona, Italy). MMTV-PyMT mice on the C57BL/6 background were kindly provided by M.P. Colombo (Fondazione IRCCS Istituto Nazionale dei Tumori, Milan, Italy). MMTV-PyMT, *Dab2*$^{flox/flox}$, *Tie2*-Cre$^+$ mice were generated in house by crossing three strains and maintained by intercross. *Yap*$^{flox/flox}$*Taz*$^{flox/flox}$ mice were kindly provided by S. Piccolo (University of Padua, Padua, Italy) and were cross-bred with *Tie2*-Cre mice to generate *Yap–Taz* KO mice. OT-1 TCR-transgenic mice (C57BL/6-Tg(TcraTcrb)1100Mjb/J) and CD45.1$^+$ congenic mice (B6.SJL-PtrcaPepcb/BoyJ) were purchased from Jackson Laboratories. All mice were maintained under specific pathogen-free conditions in the animal facility of the University of Verona. Animal experiments were performed according to national (protocol number 12722 approved by the Ministerial Decree Number 14/2012-B of January 18, 2012 and protocol number BR15/08 approved by the Ministerial Decree Number 925/2015-PR of August 28, 2015) and European laws and regulations. All animal experiments were approved by Verona University Ethical Committee and conducted according to the guidelines of Federation of European Laboratory Animal Science Association (FELASA). All animal experiments were in accordance with the Amsterdam Protocol on animal protection and welfare: mice were monitored daily and euthanized when displaying excessive discomfort.

Cell Cultures

Murine E0771 breast cancer cells derived from C57BL/6 mice (CH3 BioSystems, #94A001) were cultured in RPMI 1640 (Euroclone). Murine MN-MCA1 fibrosarcoma cell line (gift from A. Sica, Istituto Humanitas, Milan, Italy), RAW264.7 macrophage cell line (ATCC TIB-71), and SVEC4-10 endothelial cell line (gift from A. Viola, Istituto di Ricerca Pediatrica, Padua, Italy; originally obtained from ATCC CRL-2181) were cultured in DMEM (Euroclone). All media were supplemented with 10% heat-inactivated FBS (Superior, Merck), 20 μmol/L β-Mercaptoethanol (Sigma-Aldrich), 2 mmol/L L-glutamine, 10 mmol/L HEPES, 150 U/mL streptomycin, 200 U/mL penicillin/streptomycin (all from Euroclone). Cell lines were thawed from primary stocks maintained under liquid nitrogen and cultured for a maximum of 1 month (E0771, RAW264.7, and SVEC4-10) or for few passages (MN-MCA1), during which time all experiments were performed. The cultures were maintained at 37°C in 5% CO_2-humidified atmosphere and regularly tested for *Mycoplasma* using MycoAlert LookOut Mycoplasma PCR Detection Kit (Sigma-Aldrich).

Patients with Breast Cancer

To explore the prognosis (in terms of DFS) according to DAB2 expression, tumor samples with clinical annotations from a series of 32 patients affected by pure invasive lobular carcinoma (Supplementary Table S2) and surgically treated at the University Hospital of Verona, were collected. In addition, with the aim to evaluate the distribution of DAB2 according to tumor cell proliferation (by the IHC assessment of Ki-67 antigen), a series of luminal ILC was collected ($n = 30$; Supplementary Table S3). A database for individual data and information was appropriately fulfilled. The study was approved by the local Ethics Committee (Prot. CESC n° 24163, May 20, 2014).

Patients with Gastric Cancer

The potential prognostic role of DAB2 in gastric cancer was evaluated in terms of CSS and OS. Data and samples from 59 patients affected by gastric cancer who underwent surgery at the University Hospital of Verona (Verona, Italy) were collected (Supplementary Table S4). Tumor samples were available in tissue microarrays with tumor cores of each considered case and obtained from the inner part of the tumors. The study was approved by the local Ethics Committee (Prot. CESC n° 19147 November 28, 2011).

Spontaneous and Experimental Metastases Assays

For spontaneous metastasis formation, breast cancer (E0771) and fibrosarcoma (MN-MCA1) cell lines were orthotopically injected into the mammary fat pad (5×10^5 cells/mouse) and into the left quadriceps of mice (10^5 cells/mouse) respectively. Tumor growth was monitored every 2 days using a digital caliper. The greatest longitudinal diameter (length) and the greatest transverse diameter (width) were determined and tumor volume was calculated by the modified ellipsoidal formula: tumor volume = 1/2 (length × width^2). In the case of E0771-injected mice, tumors were resected at 800 mm^3 of volume, to favor distal dissemination. For experimental metastasis formation, eight-week-old WT or *Dab2* KO females were injected with 4×10^5 E0771 cells into the tail vein. Mice were euthanized 20 days after tumor cell injection and lungs were analyzed for metastasis formation. 10^6 E0771-mCherry/Luc cells were intravenously injected in WT or *Dab2* KO mice to follow metastasis seeding and growth at the metastatic site using *in vivo* bioluminescence imaging every week (IVIS Spectrum optical imager). For spontaneous tumorigenesis and metastasis studies, MMTV-PyMT female mice carrying the specific oncogenes were examined weekly for mammary tumors to define tumor incidence. Thirteen weeks after the appearance of the first tumor, mice were euthanized and lungs were analyzed for metastasis formation.

Anti–PD-1 Immunotherapy

The effect of anti–PD-1 immunotherapy was investigated in C57BL/6J mice, WT or *Dab2* KO, after an orthotopic challenge with 10^5 MN-MCA1 cells. Tumor-bearing mice with established tumor masses were treated using 4 iterative intraperitoneal administrations of anti–PD-1 mAb (clone RMP1-14; InVivoMAb) or isotype Ab (clone 2A3) every 2 days. The complete treatment consists of 1 mg of Ab. MN-MCA1–bearing mice were euthanized 25 days after tumor challenge for metastases evaluation.

CRISPR/Cas9 Gene Editing

For each DNA target coding sequence (*Dab2, Itgβ1, Itgα5, Itgα6*), three sgRNAs with the highest scores on target and lowest numbers of off-targets were chosen using the MIT CRISPR design tool (http://crispr.mit.edu/) and cloned in pSpCas9(BB)-2A-GFP (PX458) vector (Addgene), which also encoded a reporter gene (GFP) and Cas9 protein. Control digestion and Sanger sequencing were performed to evaluate the success of cloning. Plasmid transfection in RAW264.7 cells was performed with K2 reagent (Biontex). After two days, cells were collected, enriched for GFP using a FACS Aria II Flow Cytometer Cell Sorter (BD Biosciences), and cultured as single cell–derived clones. Clones were screened by protein (flow cytometry and Western blot analyses) and genetic (Sanger sequencing) analysis.

scRNA-seq

Tumors pooled from 3 PyMT-WT and 3 PyMT-*Dab2* KO mice were digested as reported above and myeloid cells were FACS-sorted as CD45$^+$ lineage (CD3, CD19, NK1.1) negative cells. Sorted cell suspension (10,000 cells, about 650 cells/μL) was loaded on a GemCode Single Cell Instrument (10x Genomics Chromium System) to generate single-cell GEMs (Gel bead-in-EMulsion). scRNA-seq libraries were prepared using GemCode Single Cell 3′ Gel Bead and Library Kit v2 (10x Genomics). Sequencing was performed using an Illumina NextSeq500 with 26 bases for Read1 and 98 bases for Read2. Demultiplexing and alignment to the Mouse mm10 genome were done with 10x Cell Ranger v3.0.2. Output for the two samples were then merged using Cell Ranger Aggr, where WT reads were downsampled to account for its slightly higher read count compared with *Dab2* KO. The resulting combined gene × cell UMI count dataset was used for downstream analysis utilizing the functions of the Seurat v3 R package (see Supplementary Information). Raw sequencing data have been deposited in the Gene Expression Omnibus (GEO) under accession number GSE152674.

Invasion Assays

In vitro invasion assays were performed using Matrigel and 8-μm pore transwells (both from Corning Inc.). BMDMs or RAW264.7 cells were resuspendend in 2% FBS growth medium and seeded on top of the polymerized Matrigel, whereas 20% FBS growth medium was added in the well as cell chemoattractant. For BMDMs, CSF1 (100 ng/mL) was added both in the underneath well and on top of the Matrigel. After 4 days, Matrigel was removed, and invading cells were fixed, stained with crystal violet, and eluted with a solution containing 50% ethanol and 0.1% acetic acid. Absorbance was measured at 595 nm using a microplate reader (VersaMax, Molecular Devices). In the invasion assay with tumor cells, BMDMs were left in culture for 3 days to remodel the matrix and killed with puromycin (5 μg/mL) for 48 hours. After several washes, E0771 cells were seeded on top of the Matrigel in 2% FBS culture medium, while 20% FBS medium was added in the underneath well. Breast cancer cell invasion ability was evaluated after 24 hours by crystal violet elution and absorbance measurement. To study the correlation between DAB2, integrins, and EMC components in the metastatic process, Puramatrix synthetic matrix (Corning Inc.) was mixed with different

amounts of fibronectin, laminin (Thermo Fisher Scientific), vitronectin, collagen I (Corning Inc.), and collagen IV (BD Biosciences), coated on 8-μm pore transwells. Invading ability was assessed by crystal violet elution after 72 hours.

Inverted Invasion Assay

Macrophage ability to remodel the ECM and to guide invasion of cancer cells was tested by *in vitro* inverted invasion assays. Breast cancer cells (E0771) and TAMs or RAW264.7 cells were labeled with CellVue (Thermo Fisher Scientific) and PKH dyes (Sigma-Aldrich), respectively, and mixed with Matrigel (Corning Inc.) on chambered cell culture slides (Thermo Fisher Scientific). After the polymerization, a layer of Matrigel mixed with 5% Collagen Type I–FITC conjugate was added on the top. Once polymerized, Matrigel was covered with complete medium, creating a chemotactic gradient. After 72 hours, 6 random fields for each condition were imaged at fixed intervals (10 μm) starting at the fluorescent layer and in a direction toward the chemotactic gradient using the *z*-stack setting of Leica TCS SP5 confocal microscope. To evaluate tumor cell invasion ability, distance travelled and invaded areas were quantified using ImageJ software.

SHG Imaging

To evaluate possible differences in ECM organization within tumors derived from WT, *Dab2* KO, and *Yap–Taz* KO mice, we took advantage of SHG to image fibrillar, cross-linked collagen in tissues. SHG signal was acquired through an 80-μm *z*-stack in fixed tumor samples, using a 25× NA 1.05 water-immersion objective (Olympus XLPLN25XWMP2) on a custom-built microscope, described in detail elsewhere (48). A 800-nm laser wavelength/395 nm ± 25 nm emission wavelength was used to collect SHG signal from collagen I fibers. Images were then analyzed for signal intensity of each single *z*-step (8-μm steps) or maximum projection intensity of *z*-stack, using ImageJ software.

In Vitro *Dab2* Induction

$CD11b^+$ cells were immunomagnetically sorted from tumor-free and MN-MCA1 tumor–bearing mice and cultured for 24 hours in the presence of serum-free growth media supplemented with CSF1 (100 ng/mL) or E0771 supernatant. Alternatively, cells were grown in coculture with previously irradiated (8,000 rad) E0771 cells. To assess whether CSF1 has a direct effect on *Dab2* gene expression, TAMs isolated from MN-MCA1 tumor-bearing mice were cultured with CSF1 (100 ng/mL) for 24 hours. To understand if *Dab2* expression is modulated by adhesion, $CD11b^+$ cells were isolated from tumor-free mice and cultured for 6 hours in adhesion on a plastic surface or in suspension. In both conditions, CSF1 or E0771 supernatant were added to the serum-free growth media. Samples were harvested for RNA isolation. *Dab2* expression was analyzed by real-time PCR and normalized on unstimulated cells.

Statistical Analyses

Student *t* test (parametric groups) and Wilcoxon–Mann–Whitney test (nonparametric groups) were used to determine statistical significance of differences between two treatment groups, and ANOVA test was used in the case of multiple comparisons. Growth curves were analyzed with repeated measures two-way ANOVA using the SAS system. Survival analysis was performed using the Kaplan–Meier survival analysis (log-rank) method. Values were considered significant at $P \leq 0.05$. Values are reported as mean ± SE or SD. All analyses were performed using Graph Pad Prism (version 8.4.2).

Statistical Analyses for Patients

Descriptive statistics was adopted. Follow-up was analyzed and reported according to Shuster and colleagues (49). DAB2 expression data were obtained from the IHC staining on patient biopsies. The ROC analysis was applied to the DAB2 continuous score to dichotomize the obtained values according to DFS for patients with ILC. To correlate DAB2 expression with clinicopathologic data, Pearson χ^2 test or Fisher exact test were used, depending on sample size. The presence of lymph node metastases, tumor cell proliferation (Ki-67 expression), and vascular invasion (V.I.) inside the primary breast tumor were considered as characteristics of interest.

DFS, CSS, and OS curves were elaborated using the Kaplan–Meier method, and significance was calculated with the log-rank test. *P* values were considered significant when ≤0.05. The SPSS 18.0, R 2.6.1, and MedCalc 14.2.1 statistical programs were used for all analyses.

For complete experimental details and reagents, please see Supplementary Methods.

Disclosure of Potential Conflicts of Interest

M. Fassan reports grants and personal fees from Astellas Pharma, grants from QED Therapeutics, and personal fees from Tesaro outside the submitted work. V. Bronte reports personal fees from Codiak BioSciences and personal fees from IO Biotech ApS outside the submitted work. No potential conflicts of interest were disclosed were disclosed by the other authors.

Authors' Contributions

I. Marigo: Conceptualization, investigation, project administration, writing-review and editing. **R. Trovato:** Conceptualization, investigation, project administration, writing-review and editing. **F. Hofer:** Conceptualization, investigation, visualization, writing-original draft, writing-review and editing. **V. Ingangi:** Investigation, methodology, writing-original draft. **G. Desantis:** Investigation, methodology. **K. Leone:** Investigation, methodology. **F. De Sanctis:** Investigation, methodology. **S. Ugel:** Investigation, writing-review and editing. **S. Cane:** Investigation, writing-review and editing. **A. Simonelli:** Formal analysis. **A. Lamolinara:** Investigation. **M. Iezzi:** Investigation, methodology. **M. Fassan:** Investigation, methodology. **M. Rugge:** Resources. **F. Boschi:** Investigation. **G. Borile:** Investigation. **T. Eisenhaure:** Formal analysis. **S. Sarkizova:** Formal analysis. **D. Lieb:** Formal analysis. **N. Hacohen:** Formal analysis, writing-review and editing. **L. Azzolin:** Resources. **S. Piccolo:** Resources, writing-review and editing. **R. Lawlor:** Resources. **A. Scarpa:** Resources. **L. Carbognin:** Methodology. **E. Bria:** Methodology, writing-original draft. **S. Bicciato:** Formal analysis, writing-review and editing. **P.J. Murray:** Resources, writing-review and editing. **V. Bronte:** Conceptualization, supervision, funding acquisition, project administration, writing-review and editing.

Acknowledgments

We thank Cristina Anselmi, Ornella Poffe, Tiziana Cestari, Giulio Fracasso, Vincenza Guzzardo, and Andrea Filippi for outstanding technical assistance; and Erich Piovan, Sara Valsoni, Isabella Sperduti, and Silvia Sartoris for reagents, bioinformatics analysis, and helpful discussion. We thank J.A. Cooper (Fred Hutchinson Cancer Center, Seattle, WA) for the gift of the *Dab2* conditional allele mice. We deeply acknowledge the contribution of 'Centro Piattaforme Tecnologiche' of the University of Verona for sorting and imaging experiments. We thank the personnel of ARC-Net Research Centre for assistance in clinicopathologic data acquisition. This work was supported by V. Bronte grants of the Italian Association for Cancer Research (18603 and 12182 that refers to Special Program Molecular Clinical Oncology 5 per mille) and by grants of the Cancer Research Institute (Clinic and Laboratory Integration Program, CLIP 2017), Cariverona Foundation (Project call, 2017), and Qatar National Priority Research Program 2017, Project: NPRP11S-1211-170086). R. Trovato was supported by AIRC/

FIRC fellowship call 2018. E. Bria is currently supported by the Associazione Italiana per la Ricerca sul Cancro (AIRC), Investigator Grant (IG) no. IG20583, and by Institutional funds of Università Cattolica del Sacro Cuore (UCSC-project D1-2018/2019). I. Marigo was supported by Euronanomed III (Joint Translational Call 2019 Project NanoNET N. 723770) and IOV 5 × 1000 Intramural Research Grant Project (N.BIGID219MARI).

Received January 10, 2020; revised June 8, 2020; accepted July 6, 2020; published first July 10, 2020.

REFERENCES

1. Steeg PS. Targeting metastasis. Nat Rev Cancer 2016;16:201–18.
2. Cassetta L, Fragkogianni S, Sims AH, Swierczak A, Forrester LM, Zhang H, et al. Human tumor-associated macrophage and monocyte transcriptional landscapes reveal cancer-specific reprogramming, biomarkers, and therapeutic targets. Cancer Cell 2019;35:588–602.
3. Steidl C, Lee T, Shah SP, Farinha P, Han G, Nayar T, et al. Tumor-associated macrophages and survival in classic Hodgkin's lymphoma. N Engl J Med 2010;362:875–85.
4. Mantovani A, Marchesi F, Malesci A, Laghi L, Allavena P. Tumour-associated macrophages as treatment targets in oncology. Nat Rev Clin Oncol 2017;14:399–416.
5. Di Caro G, Cortese N, Castino GF, Grizzi F, Gavazzi F, Ridolfi C, et al. Dual prognostic significance of tumour-associated macrophages in human pancreatic adenocarcinoma treated or untreated with chemotherapy. Gut 2016;65:1710–20.
6. Qian BZ, Li J, Zhang H, Kitamura T, Zhang J, Campion LR, et al. CCL2 recruits inflammatory monocytes to facilitate breast-tumour metastasis. Nature 2011;475:222–5.
7. Qian B, Deng Y, Im JH, Muschel RJ, Zou Y, Li J, et al. A distinct macrophage population mediates metastatic breast cancer cell extravasation, establishment and growth. PLoS One 2009;4:e6562.
8. Lin EY, Nguyen AV, Russell RG, Pollard JW. Colony-stimulating factor 1 promotes progression of mammary tumors to malignancy. J Exp Med 2001;193:727–40.
9. Cassetta L, Pollard JW. Targeting macrophages: therapeutic approaches in cancer. Nat Rev Drug Discov 2018;17:887–904.
10. Xu XX, Yang W, Jackowski S, Rock CO. Cloning of a novel phosphoprotein regulated by colony-stimulating factor 1 shares a domain with the Drosophila disabled gene product. J Biol Chem 1995;270:14184–91.
11. Xu XX, Yi T, Tang B, Lambeth JD. Disabled-2 (Dab2) is an SH3 domain-binding partner of Grb2. Oncogene 1998;16:1561–9.
12. Hocevar BA, Prunier C, Howe PH. Disabled-2 (Dab2) mediates transforming growth factor beta (TGFbeta)-stimulated fibronectin synthesis through TGFbeta-activated kinase 1 and activation of the JNK pathway. J Biol Chem 2005;280:25920–7.
13. Adamson SE, Griffiths R, Moravec R, Senthivinayagam S, Montgomery G, Chen W, et al. Disabled homolog 2 controls macrophage phenotypic polarization and adipose tissue inflammation. J Clin Invest 2016;126:1311–22.
14. Hocevar BA, Mou F, Rennolds JL, Morris SM, Cooper JA, Howe PH. Regulation of the Wnt signaling pathway by disabled-2 (Dab2). EMBO J 2003;22:3084–94.
15. Teckchandani A, Mulkearns EE, Randolph TW, Toida N, Cooper JA. The clathrin adaptor Dab2 recruits EH domain scaffold proteins to regulate integrin beta1 endocytosis. Mol Biol Cell 2012;23:2905–16.
16. Mettlen M, Loerke D, Yarar D, Danuser G, Schmid SL. Cargo- and adaptor-specific mechanisms regulate clathrin-mediated endocytosis. J Cell Biol 2010;188:919–33.
17. Chetrit D, Ziv N, Ehrlich M. Dab2 regulates clathrin assembly and cell spreading. Biochem J 2009;418:701–15.
18. Lo CM, Wang HB, Dembo M, Wang YL. Cell movement is guided by the rigidity of the substrate. Biophys J 2000;79:144–52.
19. Marigo I, Zilio S, Desantis G, Mlecnik B, Agnellini AH, Ugel S, et al. T cell cancer therapy requires CD40-CD40L activation of tumor necrosis factor and inducible nitric-oxide-synthase-producing dendritic cells. Cancer Cell 2016;30:651.
20. Ridiandries A, Tan JTM, Bursill CA. The role of chemokines in wound healing. Int J Mol Sci 2018;19:3217.
21. Hofmann HS, Hansen G, Richter G, Taege C, Simm A, Silber RE, et al. Matrix metalloproteinase-12 expression correlates with local recurrence and metastatic disease in non-small cell lung cancer patients. Clin Cancer Res 2005;11:1086–92.
22. Sha H, Zhang D, Zhang Y, Wen Y, Wang Y. ATF3 promotes migration and M1/M2 polarization of macrophages by activating tenascinC via Wnt/betacatenin pathway. Mol Med Rep 2017;16:3641–7.
23. Lawrence T, Natoli G. Transcriptional regulation of macrophage polarization: enabling diversity with identity. Nat Rev Immunol 2011;11:750–61.
24. Fiore A, Ugel S, De Sanctis F, Sandri S, Fracasso G, Trovato R, et al. Induction of immunosuppressive functions and NF-kappaB by FLIP in monocytes. Nat Commun 2018;9:5193.
25. Mossadegh-Keller N, Sarrazin S, Kandalla PK, Espinosa L, Stanley ER, Nutt SL, et al. M-CSF instructs myeloid lineage fate in single haematopoietic stem cells. Nature 2013;497:239–43.
26. Teckchandani A, Toida N, Goodchild J, Henderson C, Watts J, Wollscheid B, et al. Quantitative proteomics identifies a Dab2/integrin module regulating cell migration. J Cell Biol 2009;186:99–111.
27. Cooper J, Giancotti FG. Integrin signaling in cancer: mechanotransduction, stemness, epithelial plasticity, and therapeutic resistance. Cancer Cell 2019;35:347–67.
28. Madsen DH, Jurgensen HJ, Siersbaek MS, Kuczek DE, Grey Cloud L, Liu S, et al. Tumor-associated macrophages derived from circulating inflammatory monocytes degrade collagen through cellular uptake. Cell Rep 2017;21:3662–71.
29. Paszek MJ, Zahir N, Johnson KR, Lakins JN, Rozenberg GI, Gefen A, et al. Tensional homeostasis and the malignant phenotype. Cancer Cell 2005;8:241–54.
30. DiMilla PA, Stone JA, Quinn JA, Albelda SM, Lauffenburger DA. Maximal migration of human smooth muscle cells on fibronectin and type IV collagen occurs at an intermediate attachment strength. J Cell Biol 1993;122:729–37.
31. Cordenonsi M, Zanconato F, Azzolin L, Forcato M, Rosato A, Frasson C, et al. The Hippo transducer TAZ confers cancer stem cell-related traits on breast cancer cells. Cell 2011;147:759–72.
32. Dupont S, Morsut L, Aragona M, Enzo E, Giulitti S, Cordenonsi M, et al. Role of YAP/TAZ in mechanotransduction. Nature 2011;474:179–83.
33. Calvo F, Ege N, Grande-Garcia A, Hooper S, Jenkins RP, Chaudhry SI, et al. Mechanotransduction and YAP-dependent matrix remodelling is required for the generation and maintenance of cancer-associated fibroblasts. Nat Cell Biol 2013;15:637–46.
34. Acerbi I, Cassereau L, Dean I, Shi Q, Au A, Park C, et al. Human breast cancer invasion and aggression correlates with ECM stiffening and immune cell infiltration. Integr Biol 2015;7:1120–34.
35. Desmedt C, Salgado R, Fornili M, Pruneri G, Van den Eynden G, Zoppoli G, et al. Immune infiltration in invasive lobular breast cancer. J Natl Cancer Inst 2018;110:768–76.
36. Carbognin L, Sperduti I, Fabi A, Dieci MV, Kadrija D, Griguolo G, et al. Prognostic impact of proliferation for resected early stage 'pure' invasive lobular breast cancer: cut-off analysis of Ki67 according to histology and clinical validation. Breast 2017;35:21–6.
37. Ades F, Zardavas D, Bozovic-Spasojevic I, Pugliano L, Fumagalli D, de Azambuja E, et al. Luminal B breast cancer: molecular characterization, clinical management, and future perspectives. J Clin Oncol 2014;32:2794–803.
38. Liu J, Chen S, Wang W, Ning BF, Chen F, Shen W, et al. Cancer-associated fibroblasts promote hepatocellular carcinoma metastasis through chemokine-activated hedgehog and TGF-beta pathways. Cancer Lett 2016;379:49–59.
39. Kitamura T, Qian BZ, Pollard JW. Immune cell promotion of metastasis. Nat Rev Immunol 2015;15:73–86.
40. Lin EY, Li JF, Gnatovskiy L, Deng Y, Zhu L, Grzesik DA, et al. Macrophages regulate the angiogenic switch in a mouse model of breast cancer. Cancer Res 2006;66:11238–46.

41. DeNardo DG, Barreto JB, Andreu P, Vasquez L, Tawfik D, Kolhatkar N, et al. CD4(+) T cells regulate pulmonary metastasis of mammary carcinomas by enhancing protumor properties of macrophages. Cancer Cell 2009;16:91–102.
42. Zhu Y, Herndon JM, Sojka DK, Kim KW, Knolhoff BL, Zuo C, et al. Tissue-resident macrophages in pancreatic ductal adenocarcinoma originate from embryonic hematopoiesis and promote tumor progression. Immunity 2017;47:323–38.
43. Hung WS, Ling P, Cheng JC, Chang SS, Tseng CP. Disabled-2 is a negative immune regulator of lipopolysaccharide-stimulated Toll-like receptor 4 internalization and signaling. Sci Rep 2016;6:35343.
44. Kaplan RN, Riba RD, Zacharoulis S, Bramley AH, Vincent L, Costa C, et al. VEGFR1-positive haematopoietic bone marrow progenitors initiate the pre-metastatic niche. Nature 2005;438:820–7.
45. Costa-Silva B, Aiello NM, Ocean AJ, Singh S, Zhang H, Thakur BK, et al. Pancreatic cancer exosomes initiate pre-metastatic niche formation in the liver. Nat Cell Biol 2015;17:816–26.
46. Westcott JM, Prechtl AM, Maine EA, Dang TT, Esparza MA, Sun H, et al. An epigenetically distinct breast cancer cell subpopulation promotes collective invasion. J Clin Invest 2015;125:1927–43.
47. Anderson RL, Balasas T, Callaghan J, Coombes RC, Evans J, Hall JA, et al. A framework for the development of effective anti-metastatic agents. Nat Rev Clin Oncol 2019;16:185–204.
48. Filippi A, Dal Sasso E, Iop L, Armani A, Gintoli M, Sandri M, et al. Multimodal label-free ex vivo imaging using a dual-wavelength microscope with axial chromatic aberration compensation. J Biomed Opt 2018;23:1–9.
49. Shuster JJ. Median follow-up in clinical trials. J Clin Oncol 1991;9:191–2.